Reactivity of Deprotonated $Mn_2(\mu\text{-}H)(\mu\text{-}PCyH)(CO)_8$: Selective Monoauration to $Mn_2(\mu\text{-}AuPR_3)(\mu\text{-}PCyH)(CO)_8$ and $Mn_2(\mu\text{-}H)(\mu_3\text{-}PCy(AuPR_3))(CO)_8$ (R = Cy, Ph, *p*-C_6H_4F, *p*-C_6H_4OMe) and Kinetic Studies of Their Conversion

H.-J. Haupt,* M. Schwefer, H. Egold, and U. Flörke

Department of Inorganic and Analytical Chemistry, Universität-GH Paderborn, 33098 Paderborn, Germany

Received October 26, 1994[⊗]

In THF solution the dimanganese complex $Mn_2(\mu\text{-}H)(\mu\text{-}PCyH)(CO)_8$ (**1**) reacts with equimolar amounts of the non nucleophilic base DBU (1.8-diazabicyclo[5.4.0]undec-7-en) and $ClAuPR_3$ (R = Cy, Ph, *p*-C_6H_4OMe, *p*-C_6H_4F) at 20 °C within 1 h to afford the following mono- and diaurated pairs of isomers: $Mn_2(\mu\text{-}AuPR_3)(\mu\text{-}PCyH)(CO)_8$ (**A**) and $Mn_2(\mu\text{-}H)(\mu_3\text{-}PCy(AuPR_3))(CO)_8$ (**B**); $Mn_2(\mu\text{-}AuPR_3)(\mu\text{-}PCy(AuPR_3))(CO)_8$ and $Mn_2(AuPR_3)_2(\mu_4\text{-}PCy)(CO)_8$. Whereas we described the separated components of the last named pair in our previous publication, the monoaurated isomers are dicussed in this paper. These isomers have now been separated by a fractional crystallization procedure and identified by means of ^1H NMR, ^{31}P NMR, UV/vis, and ν(CO) IR spectroscopic measurements. In the case of R = Ph, $Mn_2(\mu\text{-}AuPPh_3)(\mu\text{-}PCyH)(CO)_8$ (**2**) and $Mn_2(\mu\text{-}H)(\mu_3\text{-}PCy(AuPPh_3))(CO)_8$ (**3**) both crystallize triclinic, space group $P\bar{1}$, $Z = 2$: **2**, $a = 10.687(2)$ Å, $b = 11.605(2)$ Å, $c = 14.369(2)$ Å, $\alpha = 103.91(1)°$, $\beta = 99.85(1)°$, $\gamma = 93.97(1)°$; **3**, $a = 12.741(1)$ Å, $b = 16.371(1)°$ Å, $c = 9.068(2)°$ Å, $\alpha = 97.86(1)°$, $\beta = 110.73(1)°$, $\gamma = 74.99(1)°$. Both molecular structures show a common edge-sharing coordination bioctahedron with an orthogonal Mn−Mn bond. Proceeding from **1**, the μ-H atom is replaced by the isolobal group $AuPPh_3$ to obtain **2** on the one hand, and on the other hand, the phosphorus bound H atom is exchanged by the same group to get **3**. The Mn−Mn bond length is 3.136(2) Å in **2** and 2.927(1) Å in **3**. In solution, **A** and **B** form a dynamic equilibrium whose displacement depends on the R groups and on the solvent used. A mechanistic pathway for the formation of **2** and **3** is proposed. In connection with this the anion $[Mn_2(\mu\text{-}PCyH)(CO)_8]^-$ **1a** is described which was obtained as the salt Li[**1a**] (yield 81%) by the reaction of PhLi and **1** in THF solution. Finally, the kinetic data for the mutual conversion of the isomer pairs **A** and **B** were obtained by UV/vis measurements in different solvents (*n*-hexane, CH_2Cl_2) at selected temperatures. The influence of solvent interactions and of electronic factors of the R groups (M, I effect) on the rate constants and the steady states, respectively, is discussed.

Introduction

In an earlier paper, we described the cluster expansion reaction of the title compound $Mn_2(\mu\text{-}H)(\mu\text{-}PCyH)(CO)_8$ **1**. The reaction of **1** with excess DBU and 2 equiv of $ClAuPR_3$ led to the enantiotropic isomers $Mn_2(\mu\text{-}AuPR_3)(\mu_3\text{-}PCy(AuPR_3))(CO)_8$ and $Mn_2(AuPPh_3)_2(\mu_4\text{-}PCy)(CO)_8$ by an isolobal exchange of the μ-H and H(μ-P) atoms by the fragment $AuPR_3$ (R = Ph, *p*-C_6H_4F, *p*-C_6H_4OMe, Cy, Et, $(CH_2)_2CN$). The equilibrium observed was dependent on the polarity of the solvent and on the electronic and steric properties of the R groups. Knowing these facts enabled us to separate the normally thermodynamically disfavored μ_3-bridged isomer in the case of R = Cy on the basis of steric control. In the case of R = Ph, the μ_4-bridged isomer was obtained, which crystallized in a racemic mixture. Apart from the enantiotropic rearrangement of both isomers in solution, the μ_4-bridged compound additionally showed a valence isomerization/topomerization process along oppositely-situated gold−manganese edges.[1] With these complications in mind, we will now report on our efforts to obtain the missing monoaurated dimanganese isomers by selective synthetic routes. In additon we will discuss the structural characterization and the mutual conversion of these isomers. These efforts may be helpful for the development of systematic syntheses of small heterometallic cluster complexes which are of interest not only on account of their catalytic properties but also in the investigation of chiral metal cores.[2−5]

Experimental Section

Infrared spectra were recorded on a Nicolet P510 FT IR spectrometer. Proton NMR and phosphorus-31 NMR spectra were taken on a Bruker AMX 300 multinuclear pulsed Fourier transform spectrometer at 300 and 121.5 M Hz, respectively, using internal tetramethylsilane and external 85% phosphoric acid, respectively, as a reference. Chemical shifts δ are given in ppm downfield from the reference. All reactions were carried out under an argon atmosphere. Tetrahydrofuran, dichloromethane, hexane, and methanol were dried according to the literature methods, distilled and stored in the presence of argon. The gold complexes $ClAuPR_3$ (R = Ph, *p*-C_6H_4F , *p*-C_6H_4OMe, Cy) were prepared according to known synthetic routes.[6]

Preparation of $Mn_2(\mu\text{-}AuPPh_3)(\mu\text{-}PCyH)(CO)_8$ (2) and $Mn_2(\mu\text{-}H)(\mu_3\text{-}PCy(AuPPh_3))(CO)_8$ (3). A yellow solution of $Mn_2(\mu\text{-}H)(\mu\text{-}PCyH)(CO)_8$ (122 mg; 0.272 mmol) **1** and 40 μL of 1,8-diazabicyclo-[5.4.0]undec-7-en (DBU) in 10 mL of THF was stirred for 1 h at room temperature. After $ClAuPPh_3$ (134 mg; 0.272 mmol) was added, the solution turned dark orange and was then stirred for another 15 min.

[⊗] Abstract published in *Advance ACS Abstracts,* October 1, 1995.

(1) Haupt, H.-J.; Schwefer, M.; Flörke, U. *Inorg. Chem.* **1995**, *34*, 292.
(2) Haupt, H.-J.; Heinekamp, C.; Flörke, U. *Inorg. Chem.* **1990**, *29*, 2955.
(3) Haupt, H.-J.; Heinekamp, C.; Flörke, U.; Jüptner, U. *Z. Anorg. Allg. Chem.* **1992**, *608*, 100.
(4) Haupt, H.-J.; Merla, A.; Flörke, U. *Z. Anorg. Allg. Chem.* **1994**, *620*, 999.
(5) Gladfelter, W. L.; Rosselet, K. J. *Cluster Complexes as Homogeneous Catalysts and Catalyst precursor in Chemistry of Metal Cluster Complexes*; Shriver, D. F., Kaesz, H. D., Adams; R. D., Eds.; VCH Publisher Inc.: New York, 1990.
(6) Brauer, G. *Handbuch der Präp. Anorg. Chemie*, 3. Aufl.; F. Enke Verlag: Stuttgart, Germany, 1981.

0020-1669/95/1334-5461$09.00/0

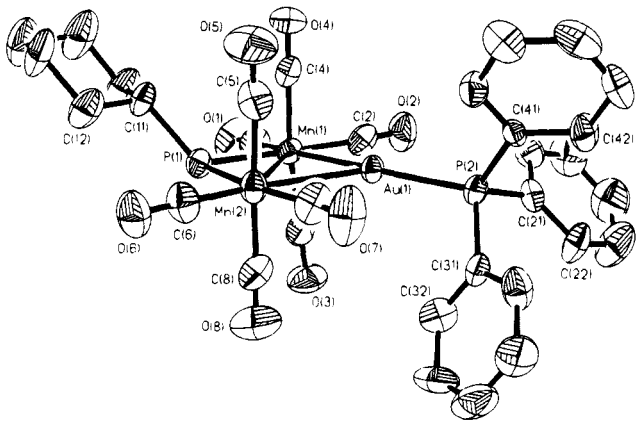

Figure 1. Molecular structure of **2**. Hydrogen atoms were omitted. ORTEP plot shows 50% probability for thermal ellipsoids.

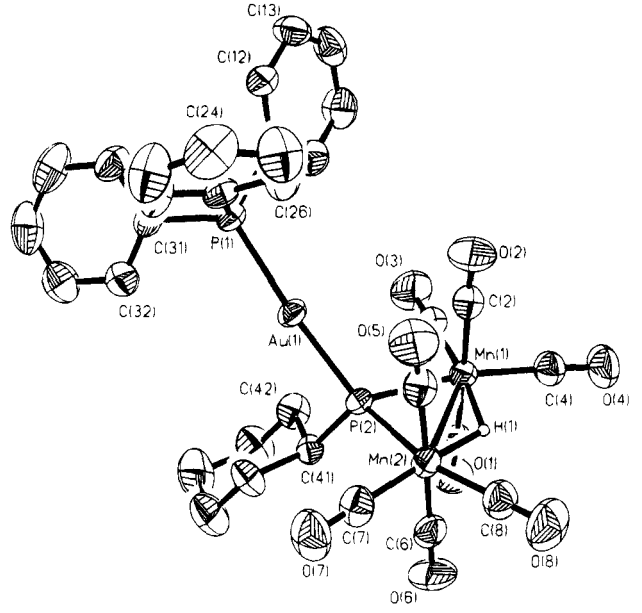

Figure 2. Molecular structure of **3**. Hydrogen atoms were omitted. ORTEP plot shows 50% probability for thermal ellipsoids.

The solvent was vacuum-stripped to leave an orange residue whose components were separated by the use of PLC plates (1 mm Silica Gel 60 F-254, Merck) and CH_2Cl_2/*n*-hexane (1:2) as eluant. The chromatogram contained three fractions (listed in order of decreasing R_f values) which were isolated and identified: first, yellow **1** (16 mg; 13%), second, orange isomers **2/3** (186 mg; 75%), and third, the red isomers $Mn_2(\mu\text{-AuPPh}_3)(\mu_3\text{-PCy(AuPPh}_3))(CO)_8$ (**4a**) and $Mn_2(AuPPh_3)_2(\mu_4\text{-PCy})(CO)_8$ (**4b**) (32 mg; 8%). The crystallization of the orange main fraction from CH_2Cl_2 solution in the presence of *n*-pentane (vapor diffusion method) made it possible to separate **2** (orange blocks) and **3** (yellow platelets). Crystals were selected by hand and were used as seed crystals to obtain further amounts of the respective compounds from supersaturated CH_2Cl_2/*n*-pentane solutions of mixtures of the isomers. The spectroscopic characterization of the complexes was achieved by IR and ^1H and ^{31}P NMR measurements. The molecular structures of **2** (Figure 1) and **3** (Figure 2) were determined by single-crystal X-ray analyses. The remaining compounds isolated from the yellow and red fraction were identified by comparing their ν(CO) IR and the ^{31}P NMR data to the corresponding data for the substances known in the literature.[1]

Data for 2 and 3. Anal. Calcd for $C_{32}H_{27}AuMn_2O_8P_2$ (M_r = 908.4): C, 42.31; H, 3.00. Found: C, 42.38; H, 3.24. IR (CH_2Cl_2), ν(CO) [cm^{-1}]: **2**, 2060 w, 2020 s, 1981 vs, 1958 s, 1931 s; **3**, 2076 w, 2043 m, 1985 vs, 1941 s. ^1H NMR ($CDCl_3$), **2** δ: 0.9−2.4 (m; 11H, Cy), 4.96 (dd; $^1J_{PH}$ = 321 Hz; $^3J_{HH(Cy)}$ = 9 Hz; 1H, H(μ-P)), 7.5−7.6 (m; 15H, PPh_3); **3** −16.12 (d; $^2J_{PH}$ = 25 Hz; 1H, μ-H), 0.9−2.4 (m; 11H, Cy), 7.5−7.6 (m; 15H, PPh_3). ^{31}P NMR ($CDCl_3$), **2**, δ: 65.1 (s; 1P, PPh_3), 163.3 (s; 1P, μ-P); proton-coupled 65.0 (s; 1P, PPh_3), 163.4 (d; $^1J_{PH}$ = 322 Hz; 1P, μ-P); **3**, 45.3 (d; $^2J_{PP}$ = 277 Hz; 1P, PPh_3), 145.5 (d; $^2J_{PP}$ = 277 Hz; 1P, μ-P).

In accord with the above synthesis, the analogous mixtures of isomers $Mn_2(\mu\text{-AuPR}_3)(\mu\text{-PCyH})(CO)_8$ **A** and $Mn_2(\mu\text{-H})(\mu_3\text{-PCy(AuPR}_3))(CO)_8$ **B** (R = Cy, *p*-C_6H_4F, *p*-C_6H_4OMe) were generated by treating $Mn_2(\mu\text{-H})(\mu\text{-PCyH})(CO)_8$ with DBU and $ClAuPR_3$. The separation procedure (chromatography and crystal selection) was the same as in the case of **2/3** (eluants used: *n*-hexane/CH_2Cl_2 15/1 (R = Cy), 1/1 (R = *p*-C_6H_4F), and 1/2 (R = *p*-C_6H_4OMe)). All isomer pairs obtained were characterized by IR and ^1H and ^{31}P NMR measurements. The molecular structures of $Mn_2(\mu\text{-AuPCy}_3)(\mu\text{-PCyH})(CO)_8$ and $Mn_2(\mu\text{-H})(\mu_3\text{-PCy(AuPCy}_3))(CO)_8$ were determined by single-crystal X-ray analyses.[15]

Spectroscopic Data for $Mn_2(\mu\text{-AuPR}_3)(\mu\text{-PCyH})(CO)_8$ A (R = Cy, *p*-C_6H_4F, *p*-C_6H_4OMe) and $Mn_2(\mu\text{-H})(\mu_3\text{-PCy(AuPR}_3))(CO)_8$ B (R = Cy, *p*-C_6H_4F, *p*-C_6H_4OMe). IR (CH_2Cl_2), ν(CO) [cm^{-1}] **A** (R = Cy), 2016 s, 1979 vs, 1950 s, 1923 s; (**A** (R = *p*-C_6H_4F)) 2022 m, 1983 vs, 1960 s, 1933 m; **A** (R = *p*-C_6H_4OMe), 2018 s, 1981 vs, 1956 s, 1931 s; **B** (R = Cy), 2074 w, 2041 m, 1981 vs, 1941 s; **B** (R = *p*-C_6H_4F), 2076 w, 2045 m, 1985 vs, 1944 vs ^1H NMR ($CDCl_3$), δ: **A** (R = Cy), 0.9−2.4 (m; 44H, Cy), 4.96 (dd, $^1J_{PH}$ = 320 Hz; $^3J_{HH(Cy)}$ = 8 Hz; 1H, H(μ-P)); **A** (R = *p*-C_6H_4F), 5.02 (dd; $^1J_{PH}$ = 332 Hz; $^3J_{HH}$ = 9 Hz, 1H, H(μ-P)), 1.2−2.4 (m; 11H, Cy), 7.1−7.7 (m; 12H, P(*p*-$C_6H_4F)_3$); **A** (R = *p*-C_6H_4OMe), 1.3−2.4 (m; 11H, Cy), 3.84 (s; 9H, Me), 4.95 (dd; $^1J_{PH}$ = 321 Hz; $^3J_{HH}$ = 9 Hz; 1H, H(μ-P)), 7.0−7.5 (m; 12H, P(*p*-$C_6H_4OMe)_3$); **B** (R = Cy), −16.11 (d; $^2J_{PH}$ = 25 Hz; 1H, μ-H), 0.9−2.4 (m; 44H, Cy); **B** (R = *p*-C_6H_4F), −16.15 (d; $^2J_{PH}$ = 25 Hz, 1H, μ-H), 1.2−2.4 (m; 11H, Cy), 7.1−7.7 (m; 12H, P(*p*-$C_6H_4F)_3$); **B** (R = *p*-C_6H_4OMe) −16.1 (d; $^2J_{PH}$ = 24 Hz, 1H, μ-H), 1.2−2.4 (m; 11H,Cy), 3.84 (s, 9H, Me), 7.0−7.5 (m; 12H, P(*p*-$C_6H_4OMe)_3$). ^{31}P NMR ($CDCl_3$), δ: **A** (R = Cy), 81.6 (s; 1P, PCy_3), 165.0 (s; 1P, μ-P); proton-coupled 81.6 (s; 1P, PCy_3), 164.7 (d; $^1J_{PH}$ = 318 Hz, 1P, μ-P); **A** (R = *p*-C_6H_4F), 63 (s (broad); 1P, P(*p*-$C_6H_4F)_3$), 164.1 (s; 1P, μ-P); proton-coupled 63 (s (broad); 1P, P(*p*-$C_6H_4F)_3$), 164.1 (d; $^1J_{PH}$ = 319 Hz; 1P, μ-P); **A** (R = *p*-C_6H_4OMe), 61.9 (s; 1P, $P(PhOMe)_3$), 163.4 (s; 1P, μ-P); proton-coupled 61.9 (s; 1P, P(*p*-$C_6H_4OMe)_3$), 163.5 (d; $^1J_{PH}$ = 327 Hz; 1P,μ-P); **B** (R = Cy), 61.9 (d; $^2J_{PP}$ = 268 Hz; 1P, PCy_3), 149.1 (d; $^2J_{PP}$ = 268 Hz; 1P, μ-P); **B** (R = *p*-C_6H_4F), 42 (s (broad); 1P, P(*p*-$C_6H_4F)_3$), 144 (s (broad); 1P, μ-P); **B** (R = *p*-C_6H_4-OMe), 41.8 (d; $^2J_{PP}$ = 285 Hz; 1P, P(*p*-$C_6H_4OMe)_3$), 146.6 (d; $^2J_{PP}$ = 283 Hz; 1P, μ-P).

Preparation of Li[$Mn_2(\mu\text{-PCyH})(CO)_8$] (Li[1a]). A solution of PhLi (125 μL; 0.200 mmol) in *n*-hexane was added to a 5 mL THF solution of **1** (100 mg; 0.222 mmol) at −90 °C. After the solution was stirred for 15 min, the cooling bath was removed and the orange-colored reaction solution reached room temperature. The solvents were vacuum-stripped to leave a yellow solid which was treated three times with *n*-pentane in order to remove **1** which did not react. Yield: 82 mg (81%).

Anal. Calcd for $C_{14}H_{12}LiMn_2O_8P$ (M_r = 456.0): C, 36.87; H 2.65. Found: C, 37.05; H, 3.87. IR(CH_2Cl_2), ν(CO) [cm^{-1}]: 2033 vw, 2020 vw, 1967 m, 1933 vs, 1910 sh, 1891 sh, 1868 sh. ^1H NMR, δ: 0.9−2.4 (m; 11H,Cy); 3.85 (dd; $^1J_{PH}$ = 329 Hz; $^3J_{HH}$ = 10 Hz; 1H, H(μ-P)). ^{31}P NMR ($CDCl_3$), δ: 133.1 (s; 1P, μ-P); proton coupled 133.1 (d, $^1J_{PH}$ = 329 Hz; 1P, μ-P).

Preparation of $Mn_2(\mu\text{-H})(\mu\text{-PCyMe})(CO)_8$. A 40 μL sample of CH_3I (0.64 mmol) was added to a solution of Li[$Mn_2(\mu\text{-PCyH})(CO)_8$] (100 mg; 0.22 mmol) in 10 mL of THF at 20 °C. The yellow solution was stirred for 20 h and afterwards evaporated to dryness. The yellow residue obtained was extracted by use of pentane to separate a mixture of **1** and the product (39 mg). In this mixture the proportion of the title compound was determined as 75% according to ^1H NMR measurements.

^1H NMR ($CDCl_3$), δ: −16.8 (d; $^2J_{PH}$ = 33 Hz; 1P, μ-H); 1.2−2.3 (m; 11H, Cy); 1.9 (d; $^2J_{PH}$ = 10 Hz; 3H, CH_3).^{31}P NMR, δ: 144.0 (s; 1P, μ-P); proton-coupled 144.0 (s; 1P, μ-P).

Kinetic UV/vis Measurements. The UV/vis data were recorded on a Lambda 15 Perkin-Elmer spectrometer by using the software PECSS. All measurements were done under an argon atmosphere. Having dissolved a portion of ca. 1.5 mg of **A** (R = Ph, Cy) in 10 mL of the respective solvent, within 2 min, the solution was poured into a cuvette of quartz glass (l = 0.5 cm). Then the measurement of intensity was immediately begun at distinct electronic absorption bands (CT-

type): **A** (R = Ph), λ = 463 nm (CH_2Cl_2); **A** (R = Cy), λ = 459 (CH_2Cl_2), 455 (*n*-hexane), 454 nm (methanol). The preparation time of each sample was noted in order to extrapolate to the initial value of the corresponding extinction E_o. During a time period of 90 min, values for the extinction E_λ were recorded every 10 s. Subsequently, the sample remained under irradiation at the respective wavelength for a further 12 h to ascertain the extinction E_λ' of the particular isomer in the equilibrium state. This radiation caused no decomposition of the compounds which was proved by comparison with extinctions of analogous solutions stored in the dark. The equations for calculating the values for the rate constants k, the equilibrium constant K_C, and the standard activation enthalpy $\Delta H^{o\#}$, entropy $\Delta S^{o\#}$, and Gibbs energy $\Delta G^{o\#}$ for the forward (k_1) and the reverse (k_{-1}) reactions were derived according to the literature.[7]

Structure Determination of 2 (Figure 1). Lattice parameters were refined from 25 reflections $11 \le 2\theta \le 25°$. Data were collected on a Siemens R3m/V diffractometer, with $\omega/2\theta$ scan, $3 \le 2\theta \le 55°$, 8115 intensities, three standards recorded every 400, only random deviations, and *Lp* and empirical absorption corrections (ψ scans); after merging (R_{int} = 0.037) there were 4690 unique observed intensities $F > 4\sigma(F)$. The structure was solved by direct and conventional Fourier methods, with full-matrix least-squares refinement based on F and 370 parameters, all but H-atoms refined anisotropically, phenyl groups treated as rigid bodies (C−C 1.395 Å), and H-atoms fixed at idealized positions. Residuals in final ΔF map were −1.36/1.08 e/Å^3 near Au position. Further information is given in Table 1. Scattering factors, structure solution, and refinement: SHELXTL-Plus.[8] Other programs: PARST.[9]

Structure Determination of 3 (Figure 2). Lattice parameters were refined from 30 reflections $17 \le 2\theta \le 30°$, with $\omega/2\theta$ scan, $3 \le 2\theta \le 55°$, and 7766 intensities. Standards were as before. Corrections and structure solution were as before. A total of 7525 independent reflections were observed (R_{int} = 0.032). Refinement was based on F^2 and 410 parameters, all but H-atoms refined anisotropically. The μ-H position was derived from a difference map and refined. Residuals in final ΔF map were −1.30/0.78 e/Å^3 near heavy atom positions. Scattering factors and structure refinement: SHELXL-93.[10] Other programs were as before.

Results and Discussion

Preparation and Selectivity. The reaction of $Mn_2(\mu\text{-}H)(\mu\text{-}PCyH)(CO)_8$ (**1**) with the nonnucleophilic nitrogen base DBU in a molar ratio of 1:1 in THF solution leads to a selective and nearly total deprotonation of the μ-H functional group within 1 h, yielding the anionic species $[Mn_2(\mu\text{-}PCyH)(CO)_8]^-$ (**1a**). This was demonstrated by a proton-coupled ^{31}P NMR spectrum which showed, apart from the signal for **1** (103.2 ppm (d; $^1J_{PH}$ = 329 Hz)), only one further signal, a doublet at 133.1 ppm ($^1J_{PH}$ = 305 Hz) for **1a**. The observed shift to low field of 29.9 ppm corresponds very well to the shift of $Mn_2(\mu\text{-}H)(\mu\text{-}PCy_2)(CO)_8$ (185 ppm) to its anion $[Mn_2(\mu\text{-}PCy_2)(CO)_8]^-$ (209 ppm).[3] Finally, when the base was added in excess (3×) the bridging hydrido atom in **1** was completely removed. This observation was the same, even after 24 h. This means that neither a conceivable dianion $[Mn_2(\mu\text{-}PCy)(CO)_8]^{2-}$ nor a possible alternative monoanion $[Mn_2(\mu\text{-}H)(\mu\text{-}PCy)(CO)_8]^-$ (**1b**) can be observed within the time scale of the NMR measurement. To separate **1a** in the solid, a THF solution of **1** was treated with an equimolar amount of PhLi at −90 °C for 30 min. After the solution warmed up to room temperature, the yellow salt $Li[Mn_2(\mu\text{-}PCyH)(CO)_8]$ (Li[**1a**]) was isolated in a yield of 81%. A ^{1}H NMR spectrum of **1a** showed no peaks in the negative ppm region which could assigned to a μ-H atom. The ^{1}H resonance of its phosphorus bound hydrogen atom was recorded as a double doublet ($^1J_{PH}$ = 329 Hz, $^3J_{HH(Cy)}$ = 10 Hz) at 3.85 ppm. In comparison to **1**, this signal exhibited only a small high-field shift ($\Delta\delta$ = 0.35). For this reason, a possible μ_3-H bonding pattern of this H atom can be excluded.

Subsequently, the anion **1a**, which was generated in situ from **1** and DBU in a molar ratio of 1:1 in THF solution, was treated with an equimolar amount of $ClAuPPh_3$. The product separation led to three fractions: first (yellow), **1** (yield 13%); second (orange), $Mn_2(\mu\text{-}AuPPh_3)(\mu\text{-}PCyH)(CO)_8$ (**2**) and $Mn_2(\mu\text{-}H)(\mu_3\text{-}PCy(AuPPh_3))(CO)_8$ (**3**) (75%); third (red), $Mn_2(\mu\text{-}AuPPh_3)(\mu_3\text{-}PCy(AuPPh_3))(CO)_8$ (**4a**) and $Mn_2(AuPPh_3)_2(\mu_4\text{-}PCy)(CO)_8$ (**4b**) (8%). The first and third fraction were identified by comparing their IR and ^{31}P NMR data.[1] A ^{31}P NMR spectrum of the main fraction contained two additional doublets (45.3 (d; $^2J_{PP}$ = 277 Hz); 145.5 (d; $^2J_{PP}$ = 227 Hz)) apart from the signals of the expected compound **2** (65.0 (s) 163.4 (s)). These additional signals were assigned to **3**, the geometrical isomer of **2** (see Figures 1 and 2). In the proton-coupled ^{31}P NMR spectrum, the signal of the μ-P atom was split to a doublet of 322 Hz, while the signals of **3** remained unchanged. The isomers **2** and **3** were separated by a fractional crystallization procedure; a crystal mixture of **2** and **3** can also be sorted by hand, based on the different crystal color and morphology. Thus the isolation of the pure isomers allowed a complete spectroscopic characterization (IR, ^{1}H NMR, ^{31}P NMR (proton coupled and decoupled)). The change of electronic and structural properties caused by the substitution of H by $AuPPh_3$ can be derived most easily from the IR data for **1**, **2**, and **3**. Thus, the pattern of the ν(CO) IR absorption modes for **3** (according to number and intensity) is nearly identical to that for **1**. The vibrations are merely shifted about 16 cm^{-1} to lower reciprocal wavelengths which is due to a higher EN (Allred and Rochow) of the H atom, compared to the group $AuPPh_3$. Consequently, the exchange of the phosphorus bound H atom by the residue $AuPPh_3$ presumably causes no steric distortion of the CO coordination sphere. In contrast, the replacement of the μ-H atom by the μ-$AuPPh_3$ group leads to a changed pattern of the relevant vibrations, a result originating from a lowering of the local symmetry of the CO ligand arrangement.[11] These structural

Table 1. Crystallographic Data for **2** and **3**[a]

	2	**3**
formula	$AuC_{32}H_{27}Mn_2O_8P_2$	$AuC_{32}H_{27}Mn_2O_8P_2$
mol wt	908.3	908.3
cryst size, mm	0.10 × 0.16 × 0.18	0.15 × 0.25 × 0.31
space group (No.)	$P\bar{1}$ (2)	$P\bar{1}$ (2)
a, Å	10.687(2)	12.741(1)
b, Å	11.605(2)	16.371(1)
c, Å	14.369(2)	9.068(2)
α, deg	103.91(1)	97.86(1)
β, deg	99.85(1)	110.73(1)
γ, deg	93.97(1)	74.99(1)
V, Å^3	1692.9	1706.5
Z	2	2
D_{calc}, g/cm^3	1.782	1.768
$F(000)$	884	884
μ, mm^{-1}	5.16	5.16
transm coeff	0.311/0.400	0.676/0.953
R, R_w[b]	0.053, 0.039	
R1, wR2[c]		0.041, 0.089

[a] For all structures, Mo Kα radiation was used at T = 296 K. [b] SHELXTL-Plus: $w = 1/\sigma^2(F) + 0.0001F^2$, $R = \sum||F_o| - |F_c||/\sum|F_o|$; $R_w = (\sum w(|F_o| - |F_c|)^2/\sum w|F_o|^2)^{1/2}$. [c] SHELXL-93: R1 = $\sum||F_o| - |F_c||/\sum|F_o|$; wR2 = $(\sum(w(F_o^2 - F_c^2)^2)/\sum(w(F_o2)^2))^{1/2}$.

(7) Wedler, G. *Lehrbuch der Physikal. Chemie*; VCH Verlagsgesellschaft: Weinheim Germany, 1985.
(8) Sheldrick, G. M. SHELXTL-Plus. Siemens Analytical X-ray Instruments Inc., Madison, WI, 1991.
(9) Nardelli, M. *Comput. Chem.* **1983**, *7*, 95.
(10) Sheldrick, G. M. SHELXL-93. Program for Crystal Structure Refinement. Univ. of Göttingen, Germany, 1993.
(11) Iggo, J. A.; Mays, M. J.; Raithby, P. R.; Henrick, K. *J. Chem. Soc., Dalton Trans.* **1984**, 633.

Table 2. Selected Bond Lengths (Å) and Angles (deg) for **2**

	Bond Lengths		
Mn1−Mn2	3.136(2)	Mn1−C4	1.846(8)
Au1−Mn1	2.643(1)	Mn2−C5	1.845(9)
Au1−Mn2	2.736(1)	Mn2−C7	1.849(9)
Au1−P2	2.323(2)	Mn1−C1	1.783(9)
Mn1−P1	2.280(3)	Mn1−C3	1.852(8)
Mn2−P1	2.269(3)	Mn2−C6	1.756(8)
Mn1−C2	1.834(8)	Mn2−C8	1.871(9)
	Bond Angles		
Mn1−Au1−Mn2	71.3(1)	Mn2−Mn1−C2	128.4(3)
Au1−Mn1−Mn2	55.7(1)	Mn2−Mn1−C1	138.3(2)
Au1−Mn2−Mn1	53.0(1)	Mn1−Mn2−C7	124.9(2)
Mn2−Au1−P2	132.3(1)	C1−Mn1−C2	93.2(4)
Mn1−Au1−P2	154.9(1)	C3−Mn1−C4	171.5(4)
Au1−Mn1−P1	102.0(1)	Au1−Mn2−P1	99.5(1)
Mn1−Mn2−P1	46.6(1)	Mn1−Mn2−C6	141.4(3)
Mn1−P1−Mn2	87.2(1)	C6−Mn2−C7	93.6(4)
Mn2−Mn1−P1	46.3(1)	C5−Mn2−C8	177.0(3)

Table 3. Selected Atomic Coordinates ($\times 10^4$) and Equivalent Isotropic Displacement Parameters ($Å^2 \times 10^3$) for **2**[a]

	x	*y*	*z*	*U*(eq)
Au(1)	1264(1)	2438(1)	4349(1)	31(1)
Mn(1)	969(1)	2941(1)	6187(1)	33(1)
Mn(2)	3621(1)	3091(1)	5541(1)	38(1)
P(1)	3022(2)	3512(2)	7016(2)	37(1)
P(2)	629(2)	1611(2)	2677(2)	32(1)
C(1)	372(8)	3064(7)	7288(6)	49(1)
O(1)	−21(6)	3123(6)	7999(5)	75(1)
C(2)	−630(8)	2526(7)	5413(6)	46(1)
O(2)	−1683(6)	2290(6)	5035(5)	62(1)
C(3)	1139(7)	1333(7)	6035(6)	43(1)
O(3)	1157(6)	334(5)	5948(5)	67(1)
C(4)	823(7)	4505(7)	6146(6)	38(1)
O(4)	682(6)	5475(5)	6148(5)	66(1)
C(5)	3390(8)	4630(8)	5468(6)	56(1)
O(5)	3320(7)	5623(6)	5495(6)	96(1)
C(6)	5264(8)	3450(8)	6025(6)	55(1)
O(6)	6351(6)	3676(6)	6358(5)	65(1)
C(7)	3850(8)	2711(7)	4260(6)	54(1)
O(7)	4125(6)	2517(6)	3513(5)	71(1)
C(8)	3763(8)	1506(7)	5584(7)	56(1)
O(8)	3887(7)	565(6)	5612(6)	90(1)

[a] Equivalent isotropic *U* defined as one-third of the trace of the orthogonalized U_{ij} tensor.

considerations are confirmed by the results of single-crystal X-ray analyses of **1**, **2**, and **3**.

Structural Descriptions. Compounds **2** and **3** crystallize in a triclinic unit cell (Table 1). Their molecular structures are presented in Figures 1 and 2; selected positional parameters of the atoms and selected bond angles and bond lengths are given in Tables 2−5.

Structure of 2. The ligand geometry of each manganese atom in this diamagnetic compound is octahedrally distorted. The ligand arrangement comprises four CO ligands, the common phosphorus and gold atoms. The central ring $Mn_2(\mu\text{-P})(\mu\text{-Au})$ in **2** is nearly planar. The eight CO ligands which are coordinated at the manganese atoms are arranged in eclipsed positions. The four-membered ring contains a transannular Mn−Mn bond, thus fulfilling the rare gas rule. Compared to the Mn−Mn bond length of 2.940(1) Å in **1**,[12] the analogous bond length of 3.136(2) Å in **2** is distinctly longer. The observed change follows an isolobal exchange of μ-H for μ-$AuPPh_3$ from **1** to **2** and originates from the kind of bridging atom in a sterically more demanding bridging group $AuPPh_3$. The afore-mentioned elongation of the Mn−Mn bond vector is accompanied by an enlargement of the subtended bond angle at the μ-P atom from 80.6(1)° in **1** to 87.2(1)° in **2**.

Table 4. Selected Bond Lengths (Å) and Angles (deg) for **3**

	Bond Lengths		
Mn1−Mn2	292.70(12)	Mn2−C6	183.7(7)
Mn1−P2	233.2(2)	Mn2−C7	180.3(6)
Mn2−P2	232.5(2)	Mn2−C8	181.7(7)
Mn1−C1	184.3(7)	Au1−P1	230.6(1)
Mn1−C2	185.6(7)	Au1−P2	231.7(1)
Mn1−C3	179.8(7)	P2−C41	186.5(6)
Mn1−C4	183.0(6)	Mn1/2−H1	167
Mn2−C5	184.9(7)		
	Bond Angles		
Mn1−P2−Mn2	77.88(6)	C5−Mn2−C6	178.4(3)
Mn2−Mn1−P2	50.97(4)	C8−Mn2−C7	97.8(3)
Mn1−Mn2−P2	51.16(4)	P1−Au1−P2	175.23(5)
Mn1−P2−Au1	115.40(6)	Au1−P2−C41	105.5(2)
Mn2−P2−Au1	122.76(7)	Mn1−H1−Mn2	122.1
C3−Mn1−C4	100.4(3)	Mn1−P2−C41	116.4(2)
C2−Mn1−C1	176.4(3)	Mn2−P2−C41	117.4(2)

Table 5. Selected Atomic Coordinates ($\times 10^4$) and Equivalent Isotropic Displacement Parameters ($Å^2 \times 10^3$) for **3**[a]

	x	*y*	*z*	*U*(eq)
Au(1)	9124(1)	2572(1)	3721(1)	37(1)
Mn(1)	7118(1)	1116(1)	975(1)	39(1)
Mn(2)	5828(1)	2351(1)	2728(1)	38(1)
P(1)	10967(1)	2545(1)	5441(2)	34(1)
P(2)	7326(1)	2481(1)	1944(2)	34(1)
C(1)	6183(5)	1548(4)	−949(8)	43(2)
O(1)	5652(4)	1784(3)	−2178(6)	69(2)
C(2)	8136(6)	664(4)	2865(9)	53(2)
O(2)	8795(5)	366(4)	3982(6)	84(2)
C(3)	8329(5)	905(4)	289(8)	53(2)
O(3)	9111(5)	789(4)	−118(8)	88(2)
C(4)	6641(5)	125(4)	333(8)	51(2)
O(4)	6331(5)	−489(3)	−105(6)	76(2)
C(5)	6913(6)	2009(4)	4649(8)	51(2)
O(5)	7556(5)	1837(4)	5861(6)	78(2)
C(6)	4770(5)	2713(4)	820(9)	50(2)
O(6)	4096(4)	2948(4)	−354(6)	77(2)
C(7)	5551(6)	3414(4)	3575(8)	53(2)
O(7)	5382(5)	4086(3)	4097(7)	81(2)
C(8)	4744(6)	1980(4)	3156(8)	54(2)
O(8)	4066(5)	1766(4)	3462(8)	89(2)

[a] Equivalent isotropic *U* defined as one-third of the trace of the orthogonalized U_{ij} tensor.

Furthermore, the difference between the two Mn−Au bond lengths of 2.643(1) and 2.736(1) Å is striking. This feature is connected with the different Mn−Au−P bond angles of 132.3(1) and 154.9(1)°, whose difference probably originates from crystal packing forces.

Structure of 3. Corresponding to isomer **2**, **3** is also a coordination bioctahedron with one shared edge and an orthogonal Mn−Mn bond vector. The changed substitution pattern from **2** to **3** for one of the two bridging sites and the μ-P atom has the following consequences: (i) the Mn−Mn bond length of 2.927(1) Å is shortened by 0.209(2) Å compared to that of **2**; (ii) the Mn−P bond lengths (average 232.9(2) Å) exhibit no significant differences and are elongated with respect to those of **2**; (iii) the subtended bond angle at the μ-P atom of 77.9(1)° is reduced by about 9.3(1)°; (iv) there are only small differences in the Au−P bond lengths (2.306(1) and 2.317(1) Å). All these structural effects originate mainly from various electronic requirements of the changed ligands H and $AuPPh_3$ at the different coordination sites in **2** and **3**. Finally, observation iv indicates a possible electron density shift from the bridging phosphorus atom via the gold atom to the ligand PPh_3.

Properties. If crystals of **2** or **3** are dissolved in deuterochloroform, the ^{31}P NMR and ^1H NMR measurements always

(12) Flörke, U.; Schwefer, M.; Haupt H.-J. *Z. Kristallogr.* **1994**, *209*, 999.

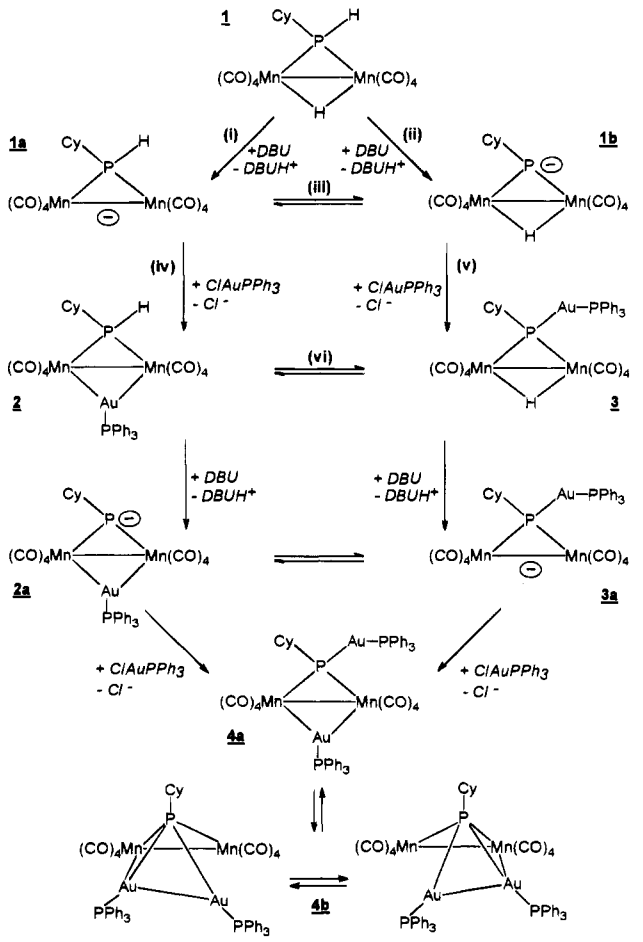

Figure 3. Reacion scheme of the deprotonation and auration of **1**.

indicate the additional existence of the other isomer in the course of time. This must be attributed to a reversible conversion of **2** and **3**. The mechanistic pathway for the deprotonation and auration of **1** up to the formation of the diaurated products **4a** and **4b** including the above-mentioned equilibrium is proposed in Figure 3.

As mentioned before, the reaction of **1** with DBU afforded the anion **1a**, which was deduced from the corresponding ^{31}P NMR spectrum. Nevertheless, it must be supposed that the abstraction of the phosphorus bound H atom is the preferred initial step. This conclusion can be reached on the basis of ^{31}P NMR spectra of the THF reaction solution of **1**, DBU and $ClAuPPh_3$ (molar ratio 1:1:1). These experiments show initially a bigger proportion of **3** than of **2** , while later on the amount of **3** decreases in favor of **2** until an equilibrium concentration of much more **2** than **3** is reached. Hence, intermediate formation of **1b** must be assumed (Figure 3(ii)), although this species cannot be detected on the time scale of the NMR experiment. However, it should be mentioned that a simultaneous direct deprotonation of the μ-H function cannot be excluded, as this pathway is known for compounds like $Mn_2(\mu\text{-}H)(\mu\text{-}PR_2)(CO)_8$ (R = Ph, Cy).[3,14] The μ-H deprotonation of this complex ($k_1 = (2.47 \pm 0.26) \times 10^{-2}$ L mol^{-1} s^{-1} for R = Cy) proceeds about 6 times more slowly than deprotonation of **1** ($k_1 = (14.03 \pm 1.34) \times 10^{-2}$ L mol^{-1} s^{-1}).[13] Consequently, **2** is preferentially generated through conversion of **3** and is generated much more slowly by means of a direct auration of **1a** (see Figure 3: kinetically favored pathway **1** (ii), **1b** (v), **3** (vi), **2**). If there is no electrophilic reactant like $ClAuPPh_3$ present in solution the anion **1b** shifts its negative ionic charge from the μ-P atom to the dimanganese fragment to become thermodynamically more stable; the ^{31}P NMR spectrum shows **1a** as the unique anion. When an equimolar amount of $ClAuPPh_3$ is added to a solution of **1a**, a ^{31}P NMR spectrum indicates signals due to **2** almost exclusively, while the formation of **3** and a decrease of **2** is detected later on. The conversion from **1a** to **1b** was proved by reaction of Li[**1a**] with methyl iodide which resulted in the P-methylated species $Mn_2(\mu\text{-}H)(\mu\text{-}PCyMe)(CO)_8$ (see Experimental Section). That is why an equilibrium between **1a** and **1b** is formulated in Figure 3. Whereas the site exchange of the H atom in the anions **1a** and **1b** could not be observed on the time scale of the ^{31}P NMR method, both of the analogous anions $[Mn_2(\mu\text{-}AuPPh_3)(\mu\text{-}PCy)(CO)_8]^-$ (**2a**) and $[Mn_2(\mu_3\text{-}PCy(AuPPh_3))(CO)_8]^-$ (**3a**) could be detected in the NMR experiment, since they need a higher activation energy because of their isolobal groups $AuPPh_3$. The anions were identified by two singlets at 62.0 and 250.4 ppm in the case of **2a**, and by two doublets at 43.7 ppm ($^2J_{PP} = 246$ Hz) and 167.9 ppm ($^2J_{PP} = 239$ Hz) in the case of the isomer **3a** when **1**, DBU, and $ClAuPPh_3$ were combined in THF solution in equivalent amounts. Finally, it should be mentioned that Figure 3 shows a simplified mechanism because possible intermolecular trans-auration processes have not been considered in it. Thus for example, **2** or **3** were observed to react with DBU alone to yield **1a** and **4a/4b** as the main products.

Table 6. Molar Fractions for **A/B** (R = Cy, Ph, p-C_6H_4F, p-C_6H_4OMe) in CH_2Cl_2 at T = 293 K (Equilibrium State)

	R = Cy	R = p-C_6H_4OMe	R = Ph	R = p-C_6H_4F
x_A	0.694	0.853	0.927	0.969
x_B	0.306	0.147	0.073	0.031

Table 7. Molar Fractions for **A/B** (R = Cy) in Selected Solvents at T = 298 K (Equilibrium State)

solvent	polarity[a]	x_A	x_B
n-hexane	0.00	0.869	0.131
dichloromethane	0.42	0.688	0.312
methanol	0.95	0.551	0.449

[a] Polarity according to Hildebrand's scale.

Influences on the Equilibrium Positions. The equilibrium position for **2** and **3** was investigated with regard to its dependency on the nature of the PR_3 groups attached to the Au atom. For this purpose **1** was treated with DBU and $ClAuPR_3$ (R = Cy, p-C_6H_4F, p-C_6H_4OMe) to generate the corresponding isomers $Mn_2(\mu\text{-}AuPR_3)(\mu\text{-}PCyH)(CO)_8$ (**A**) and $Mn_2(\mu\text{-}H)(\mu_3\text{-}PCy(AuPR_3))(CO)_8$ (**B** (R = Cy, p-C_6H_4F, p-C_6H_4OMe)). Having isolated the particular mixtures of isomers, the compounds were stirred in dichloromethane solution until the equilibrium state was reached (controlled by ^{31}P NMR). Integration of the ^{31}P resonance signals of the respective PR_3 groups led to the molar fractions x_A and x_B of each isomer (Table 6). The accuracy of the application of this method could be proved by UV/vis measurements in the case of R = Cy and Ph (see Tables 8 and 9). As evident in Table 6 the isomer of type **A** is dominant in the equilibrium state for all R groups. The formation of this type is obviously supported by an electronic withdrawing effect of the groups R. An explanation can be given in terms of the different structures of the isomers **A** and **B**. The gold(I) atom in the **A** type has a coordination number (cn) of 3 (Au, 16 VE), whereas the **B** type has a cn of 2 (Au, 14 VE). Hence the former coordination allows a better electronic saturation than the latter.

Corresponding to this idea, the equilibrium positions should also be dependent on the donor ability or the polarity of the solvent used. To evaluate this influence, solutions were

(13) Haupt, H.-J.; Egold, H. Unpublished results.
(14) Lothert, T. Dissertation, Universität-GH Paderborn, 1994.

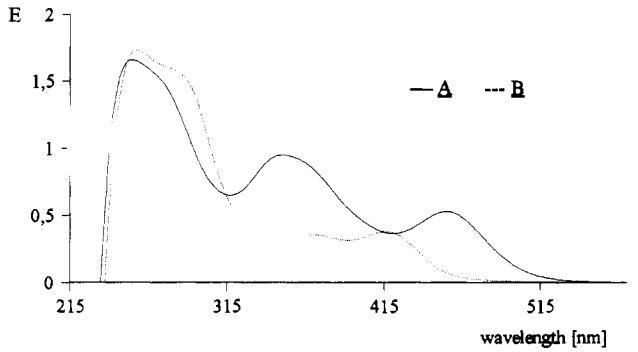

Figure 4. UV/vis spectra of **A** (R = Cy) for c = 1.82 × 10^{-4} mol L^{-1} and **B** (R = Cy) for c = 1.64 × 10^{-4} mol L^{-1} recorded in CH_2Cl_2 at T = 298 K.

Table 8. Kinetic Parameters for Isomerization of **A/B** (R = Cy) in Different Solvents at Selected Temperatures[a]

solvent	T, K	k_1, 10^{-5} s^{-1}	k_{-1}, 10^{-5} s^{-1}	K_C	x_A/x_B	r^2
CH_2Cl_2	288	2.52	5.84	0.432	0.698/0.302	0.999
CH_2Cl_2	293	4.43	10.05	0.441	0.694/0.306	0.999
CH_2Cl_2	298	7.30	16.11	0.453	0.688/0.312	0.999
CH_2Cl_2	303	11.73	26.78	0.438	0.695/0.305	0.999
n-hexane	298	0.39	2.58	0.150	0.869/0.131	0.999
n-hexane	303	0.80	5.36	0.150	0.869/0.131	0.998
n-hexane	308	1.67	11.21	0.149	0.870/0.130	0.998

[a] Limits of errors: k_1/k_{-1}, $<\pm 1 \times 10^{-7}$ s^{-1}; $K_c(CH_2Cl_2)$, $<\pm 2 \times 10^{-3}$; K_c(*n*-hexane), $<\pm 3 \times 10^{-3}$.

Table 9. Kinetic Parameters for Isomerization of **A/B** (R = Ph) in CH_2Cl_2 at Selected Temperatures

solvent	T, K	k_1, 10^{-5} s^{-1}	k_{-1}, 10^{-5} s^{-1}	K_C	x_A/x_B	r^2
CH_2Cl_2	293	0.16	2.04	0.078	0.927/0.073	0.969
CH_2Cl_2	298	0.41	5.20	0.079	0.926/0.074	0.998
CH_2Cl_2	303	0.71	7.76	0.091	0.923/0.077	0.998

[a] Limits of errors: k_1/k_{-1}, $<\pm 1 \times 10^{-7}$ s^{-1}; $K_c(CH_2Cl_2)$: $<\pm 1 \times 10^{-3}$.

investigated by UV/vis measurements, because this method requires only a very small solubility of the respective compounds. The UV/vis spectra of **A** and **B** (R = Cy) in dichloromethane are displayed in Figure 4; the corresponding values for the extinction coefficients ϵ [m^2 mol^{-1}] (λ [nm]) are given as follows: **A** (R = Cy), 910.0 (243), 521.5 (350), 290.0 (459); **B** (R = Cy), 1055.0 (239), 231.1 (415). Since **A** (R = Cy) shows a separate electronic absorption band at 459 nm, the experiments were run in dichloromethane under irradiation with this wavelength. From these measurements, the equilibrium positions **A** and **B** were determined in *n*-hexane (λ = 455 nm) and methanol (λ = 454 nm) solutions. The results (Table 7) show that the proportion of the isomer **B** rises with an increase in the solvents' polarity. Solvation interactions between molecules of the polar solvents and the **B** type isomer (cn(Au) = 2) are especially efficient and, therefore, contribute to a stabilization of **B**, even though the isomer **A** (higher intramolecular bond energy) always remains the main component at equilibrium.

Kinetic Description of the Isomerization Processes. The above discussion of the particular equilibrium shifts was based on electronic (thermodynamic) features such as bond energies and solvent interactions. To confirm these considerations, the isomerization processes **A/B** (R = Ph, Cy) were observed by UV/vis kinetic measurements to get the corresponding rate constants and activation parameters. As is generally expected for this type of intramolecular conversion, it was presumed that

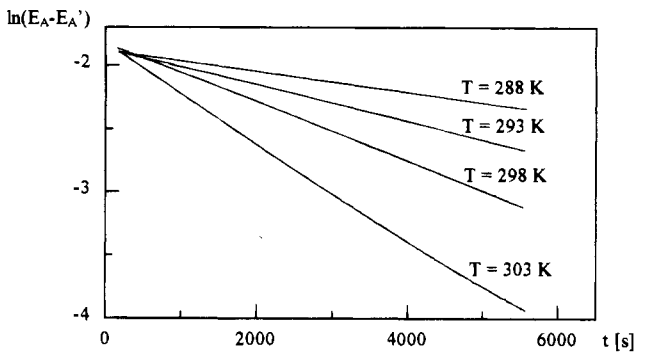

Figure 5. Plot of $\ln(E_A - E_A')$ vs t for isomerization of **A/B** (R = Cy) in CH_2Cl_2 at selected temperatures.

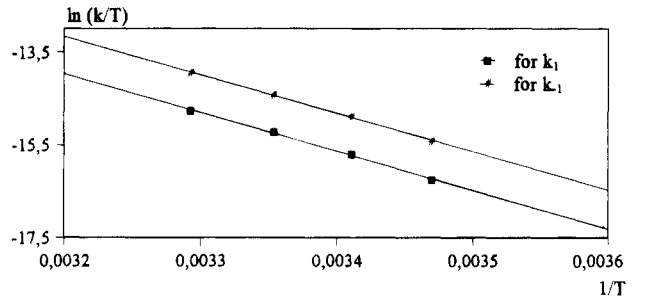

Figure 6. Plot of $\ln(k_{1/-1}/T)$ vs T^{-1} for isomerization of **A/B** (R = Cy) in CH_2Cl_2.

Table 10. Activation Parameters for Isomerization of **A/B** (R = Cy) in Dichloromethane and *n*-Hexane

	dichloromethane	*n*-hexane
$\Delta H^{\circ\#}(k_1)$, kJ mol^{-1}	72 ± 1.5	109 ± 1.2
$\Delta S^{\circ\#}(k_1)$, J mol^{-1}	−84 ± 5.0	18 ± 4.0
$\Delta G^{\circ\#}(k_1)$, kJ mol^{-1}	97 ± 2.1	104 ± 1.7
$r^2(k_1)$	0.998	0.999
$\Delta H^{\circ\#}(k_{-1})$, kJ mol^{-1}	71 ± 1.1	110 ± 1.4
$\Delta S^{\circ\#}(k_{-1})$, J mol^{-1}	−80 ± 4.0	36 ± 4.6
$\Delta G^{\circ\#}(k_{-1})$, kJ mol^{-1}	95 ± 1.6	99 ± 2.0
$r^2(k_{-1})$	0.999	0.999

the isomerization would obey a first-order rate law for both directions. The **A/B** conversions were investigated for R = Cy in dichloromethane (T(K) = 288, 293, 298, 303) and *n*-hexane (T (K) = 298, 303, 308) and for R = Ph in dichloromethane (T (K) = 293, 298, 303). The values obtained for the rate constants k_1 and k_{-1}, the equilibrium constant K_C, the correlation coefficient, and the molar fractions x_A/x_B of the isomerization process **A/B** are specified in Table 8 (R = Cy) and Table 9 (R = Ph). The corresponding activation parameters, standard activation enthalpy $\Delta H^{\circ\#}$, entropy $\Delta S^{\circ\#}$ and Gibbs energy $\Delta G^{\circ\#}$ are found in Table 10. The plots $\ln(E_A - E_A')$ vs t (Figure 5) and $\ln(k_{1/-1}/T)$ vs T^{-1} (Figure 6) illustrate the isomerization process **A/B** (R = Cy) in dichloromethane.

As indicated by the r^2 values (Tables 8 and 9), the isomerization process **A/B** obeys the first-order rate law presumed. For all temperatures investigated, the isomerization **A** to **B** and **B** to **A** runs faster in the case of R = Cy than in the case of R = Ph.

Thus the results of the kinetic investigation fit well with the thermodynamic treatment of the equilibrium positions and shifts, respectively (see Influences on the Equilibrium Positions). The better acceptor ability of the $AuPR_3$ groups (R = Ph > R = Cy) favors a bigger proportion of the **A** type compound by rendering the rearrangement of this isomer more difficult. In other words, k_1 is lowered corresponding to an increase of the relative strength of the Mn−Au bonds. Indeed, the σ Mn−Au bond lengths in **A** were observed to be somewhat shortened

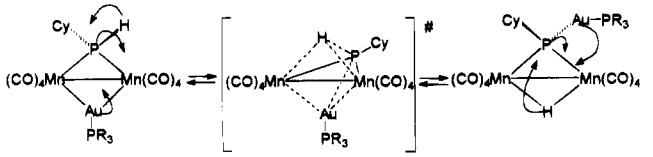

Figure 7. Mutual rearrangement of **A** and **B**.

from 2.700(2) Å for R = Cy[15] down to 2.690(1) Å for R = Ph. (The low rate of conversion for R = Ph along with the extreme equilibrium position leads to larger relative errors for k_1 and k_{-1}. Therefore, the activation parameters for R = Ph are erroneous and are not listed here.)

The influence on the rate constants of the solvents used was kinetically investigated for R = Cy in dichloromethane (288, 293, 298, and 303 K) and in *n*-hexane solution (298, 303 and 308 K). Going from dichloromethane to the less polar n-hexane the rate of conversion is distinctly reduced (Table 8). The standard activation Gibbs energy $\Delta G^{\circ\#}$ rises from 97 to 104 kJ/mol for the forward reaction (k_1) and from 95 to 99 kJ/mol for the reverse reaction (k_{-1}). This is due to an increase of the activation enthalpy $\Delta H^{\circ\#}$ (Table 9) going from CH_2Cl_2 to *n*-hexane. Conversely, the standard activation entropy $\Delta S^{\circ\#}$ alters from −84 to +18 J/molK for k_1 and from −80 to +36 J/molK for k_{-1}. Regarding this change in entropy, the transition state and its sheat of solvent molecules must be of a lower order in the case of *n*-hexane. Obviously, the transition state is of a relatively polar nature as it is stabilized by polar solvents. Thus the different $\Delta S^{\circ\#}$ values in CH_2Cl_2 compared to hexane could suggest a dissociative mechanism in the more polar solvent. However, this consideration seems very unlikely as compound **1** and the diaurated complexes **4a** and **4b** (see Figure 3) which would result from intermolecular transauration processes do not rise from the isomerization process **A/B**.

A proposal for the ligand arrangement in the transition state is presented in Figure 7. The first-order intramolecular isomerization process involves an interchange of the isolobal groups H^+ and $AuPR_3^+$ caused by the rupturing of Au−Mn, Au−P and P−H bonds. If we remember that the fission of the P−H bond needs 322 kJ/mol,[16] the $\Delta H^{\circ\#}$ values from 71 to 110 kJ/mol (Table 10) suggest a concerted rupture and formation of these bonds. The formation of the transition state can be initiated by a rocking mode which shifts the Au atom in the direction of the μ_2-P atom, on the one hand, and the μ-H atom to the μ_3-P atom, on the other.

Supporting Information Available: Part A, containing kinetic data, including (1) text giving equations for calculation of k_1, k_{-1} and K_C, $\Delta H^{\circ\#}$, $\Delta S^{\circ\#}$ and $\Delta G^{\circ\#}$ and (2) tables of UV/vis data listed for each experiment (wavelength λ, temperature T, weight of the sample m, concentration c_o, number of data points, initial extinction, slope a and intersection b of the linear regression procedure of $\ln(E - E')$ vs t or $\ln(k_{1/-1}/T)$ vs T^{-1} with their particular errors $F(a)$ and $F(b)$, average error of the single values $F(\ln(E - E'))$ and correlation coefficient r) and part B; Structural data with listings of complete atomic coordinates, bond distances and angles, anisotropic displacement parameters, and hydrogen atom coordinates for **2** and **3** (16 pages). Ordering information is given on any current masthead page.

IC941228O

(15) Flörke, U.; Haupt, H.-J. *Z. Kristallogr.* **1995**, *210*, 471.
(16) Cottrell, T. L. *The Strength of Chemical Bonds*; Butterworths: London 1958.